

ELECTRON IRRADIATION OF KUIPER BELT SURFACE ICES: TERNARY N₂–CH₄–CO MIXTURES AS A CASE STUDY

Y. S. KIM AND R. I. KAISER

Department of Chemistry, University of Hawaii at Manoa, Honolulu, HI 96822, USA; ralfk@hawaii.edu

Received 2012 June 28; accepted 2012 August 24; published 2012 September 24

ABSTRACT

The space weathering of icy Kuiper Belt Objects was investigated in this case study by exposing methane (CH₄) and carbon monoxide (CO) doped nitrogen (N₂) ices at 10 K to ionizing radiation in the form of energetic electrons. Online and in situ Fourier transform infrared spectroscopy was utilized to monitor the radiation-induced chemical processing of these ices. Along with isocyanic acid (HNCO), the products could be mainly derived from those formed in irradiated binary ices of the N₂–CH₄ and CO–CH₄ systems: nitrogen-bearing products were found in the form of hydrogen cyanide (HCN), hydrogen isocyanide (HNC), diazomethane (CH₂N₂), and its radical fragment (HCN₂); oxygen-bearing products were of acetaldehyde (CH₃CHO), formyl radical (HCO), and formaldehyde (H₂CO). As in the pure ices, the methyl radical (CH₃) and ethane (C₂H₆) were also detected, as were carbon dioxide (CO₂) and the azide radical (N₃). Based on the temporal evolution of the newly formed products, kinetic reaction schemes were then developed to fit the temporal profiles of the newly formed species, resulting in numerical sets of rate constants. The current study highlights important constraints on the preferential formation of isocyanic acid (HNCO) over hydrogen cyanide (HCN) and hydrogen isocyanide (HNC), thus guiding the astrobiological and chemical evolution of those distant bodies.

Key words: astrobiology – astrochemistry – cosmic rays – Kuiper Belt: general – methods: laboratory – planets and satellites: surfaces

Online-only material: color figures

1. INTRODUCTION

Nitrogen (N₂)-rich methane (CH₄) and carbon monoxide (CO) ices have been detected on the surface of Kuiper Belt Objects (KBOs) such as Pluto (Gulbis 2011; Schaller & Brown 2007). Douté et al. (1999) recorded near-infrared (IR) spectra of Pluto's surface and derived a nitrogen-dominated composition with a N₂:CH₄:CO ratio of about 100:0.5:0.2; methane-enriched nitrogen ices holding up to 3% methane were also reported (Tegler et al. 2010). Similar in size to Pluto (Sicardy et al. 2011), Eris was suggested to reflect surface features of methane in the visible and near-infrared ranges with the methane fraction reaching 10% in nitrogen (Tegler et al. 2010; Alvarez-Candal et al. 2011). Furthermore, Neptune's largest satellite, Triton (presumably a captured KBO), was suggested to retain a nitrogen-rich surface composition of N₂:CH₄:CO (100:0.1:0.05) close to Pluto; on Triton, traces of carbon dioxide (CO₂) and water (H₂O) ices were also suggested (Quirico et al. 1999; Grundy et al. 2010). Considering the lack of any magnetic fields, the surfaces of KBOs can be easily exposed to charged particles from the solar wind, as well as from the galactic cosmic radiation field. As demonstrated by Cooper et al. (2003), galactic cosmic ray (GCR) particles could penetrate up to meters in depth, thus chemically modifying the pristine ice composition. Most importantly, surface processing by ionizing radiation can also lead to diverse colors of KBOs (Cooper et al. 2003) in the visible range of the electromagnetic spectrum, as reported as follows. Luu & Jewitt (1996) attributed the color diversity of KBOs to a timely competition between cosmic-ray bombardment and collisional resurfacing. Meanwhile, Tegler et al. (2003) classified bimodal surface colors of KBOs into dynamic classes of primordial origin, distinguishing classical KBOs in red from others in gray. Applying the previous volatile loss model (Schaller & Brown 2007), Brown et al. (2011) coupled the current color diversity

of the Kuiper Belt with a stepwise process, which took place in the past, of a gradient evaporation of surface volatiles followed by photon and particle irradiation of remaining ices.

What is known about the radiolysis of KBO-model ices in the laboratory? Bohn et al. (1994) pioneered the ternary N₂–CH₄–CO ice processing intended to simulate the influence of solar photons on Pluto and Triton. Besides methyl radical (CH₃), ethane (C₂H₆), and carbon dioxide (CO₂), an array of products were readily observable in photolyzed ices, including diazomethane (CH₂N₂), the formyl radical (HCO), and formaldehyde (H₂CO). Moore & Hudson (2003) utilized 800 keV H⁺ beams to irradiate the ternary ice mixture (100:1:1), more closely resembling the space weathering of Pluto and Triton surface levels. The newly formed species were found to be cumulative of those found in binary ice systems: N₂–CH₄, CO–CH₄, and N₂–CO. In particular, the formation of carbon-based acids—hydrogen cyanide (HCN), hydrogen isocyanide (HNC), and isocyanic acid (HNCO)—was further suggested as a proxy to the prebiotic evolution of those distant bodies. Most recently, Fulvio et al. (2010) irradiated water-(H₂O) embedded volatile ices with 200 keV protons and monitored dosage-dependent water decays in near-IR ranges. Radiation dosages as low as about 3 eV molecule⁻¹ turned out to be sufficient to destroy as much as 80% of an initial value from matrices.

To the best of our knowledge, however, these literature data have not much utilized the scheme of an online and in situ infrared spectroscopy, as they should for extracting non-equilibrium effects of KBO volatile ices under ionizing radiation and realistic rate constants to be exploited in models of the surface processing of KBOs. Also lacking was the direct utility of energetic electrons as a radiation source that mimics those ubiquitously found either in the magnetospheres of giant planets or in the track of GCR particles (Bennett et al. 2005; Barnett et al. 2012). In this respect, the current ternary ice study

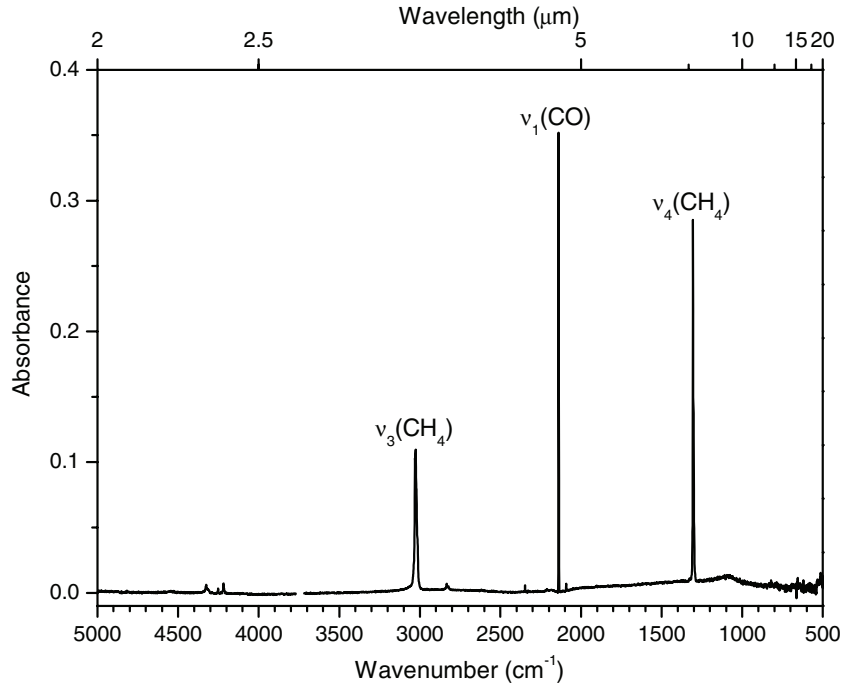


Figure 1. Mid-infrared spectrum of the ternary nitrogen, methane, and carbon monoxide ice deposited at 10 K ($\text{N}_2:\text{CH}_4:\text{CO} = 60:1:1$). The peak assignments are compiled in Table 1. Note that atmospheric contributions at about 3750 cm^{-1} were removed from the spectrum for clarity.

of KBO analog ices—nitrogen (N_2)-rich methane (CH_4) and carbon monoxide (CO)—is intended to fill in the void from reported laboratory studies. Over the past years, employing the efficient detection scheme, we have elucidated not only the production rates of new species but also the kinetics and reaction mechanisms that underlie, for example, the binary ice processing of $\text{CO}-\text{CH}_4$ (Bennett et al. 2005) and N_2-CO (Kim et al. 2011). The radiation source of 5 keV electrons was elected to deliver a few keV μm^{-1} linear energy transfer (LET) to the ice target, which is the same order of LETs that MeV GCR particles can deliver upon penetrating interstellar ices (Bennett et al. 2005). Furthermore, the current study would serve as a guide for better interpreting future field data from the *New Horizon* spacecraft (NASA) due to arrive at Pluto and Charon’s orbits in the year 2015.

2. EXPERIMENTAL

The experiments were carried out in a contamination-free ultrahigh vacuum (UHV) stainless steel chamber as described in Bennett et al. (2004). The UHV chamber can reach pressures down to 5×10^{-11} torr by a magnetically suspended turbo molecular pump that is backed by a scroll pump. All pumps used are oil free to ensure that no hydrocarbon contaminants enter the system. Temperatures down to 10 K are reached within one hour using a two-stage closed-cycle helium refrigerator that is interfaced with a feedthrough for a programmable temperature controller and also with a polished silver mirror onto which the ices are condensed. The substrate is held at the bottom of a rotary platform, which is centered in the main chamber. In this way, the temperature of the silver crystal can be regulated with a precision of ± 0.3 K between 10 K and 330 K. Gases are introduced to the main chamber via a precision leak valve, which is coupled with a linear transfer mechanism that allows a glass capillary array to be aligned 5 mm away from the substrate held at 10 K. Premixed gases of $\text{N}_2:\text{CH}_4:\text{CO}$ (60:1:1) were then condensed for eight minutes at a pressure of 1.0×10^{-7} torr.

Figure 1 depicts a mid-infrared spectrum of $\text{N}_2-\text{CH}_4-\text{CO}$ ices as deposited at 10 K. Visible in the spectrum are three prominent features of CH_4 and CO fundamentals, while any pristine ice features of homonuclear $\nu_1(\text{N}_2)$ at 2328 cm^{-1} (Jamieson & Kaiser 2007), crystalline ν_3/ν_4 (CH_4) at about $3005/1300\text{ cm}^{-1}$ (Bennett et al. 2006), or lattice vibration $\nu_1 + \nu_L$ (CO) at about 2200 cm^{-1} , have vanished (Jamieson et al. 2006). Selected overtones and combinations were traceable in the baseline and complied with reference to literature values (Table 1). Ice thickness is determined to be 400 ± 100 nm by comparing with Jamieson & Kaiser (2007) the amount of N_2 molecules condensed onto and recovered back from the substrate given a blank run.

The ice sample was then irradiated isothermally with 5 keV electrons at a nominal beam current of 0 (blank) and 100 nA. The beam has an extraction efficiency of 78.8% and is scanned over the sample area of $1.8 \pm 0.3\text{ cm}^2$. Note that actual extraction efficiency of the electron gun (Specs EQ 22–35) is stated to be 78.8%, thus correcting the fluence down to 9.8×10^{14} electrons cm^{-2} , hitting the target at a nominal current of 100 nA over 60 minutes. The radiation-induced chemical processing was then monitored by a Nicolet infrared spectrometer in a spectral range of $6000-500\text{ cm}^{-1}$. Each spectrum was online and in situ recorded in an absorption–reflection–absorption mode with a reflection angle of $\alpha = 75^\circ$, having an integrated time of 2.5 minutes, and a resolution of 2 cm^{-1} (Bennett et al. 2004). After the irradiation is complete, the ices are kept isothermally for 60 minutes before being heated to 300 K with a gradient of 0.5 K minute^{-1} .

3. INFRARED SPECTROSCOPY

We will first investigate the radiation-induced formation of new species in $\text{N}_2-\text{CH}_4-\text{CO}$ ices. Figure 2 displays the infrared spectra of ternary ices recorded at 10 K before (lower trace) and after (upper trace) the 60 minute irradiation at $0.1\ \mu\text{A}$. The electron exposure at 10 K leads to multiple

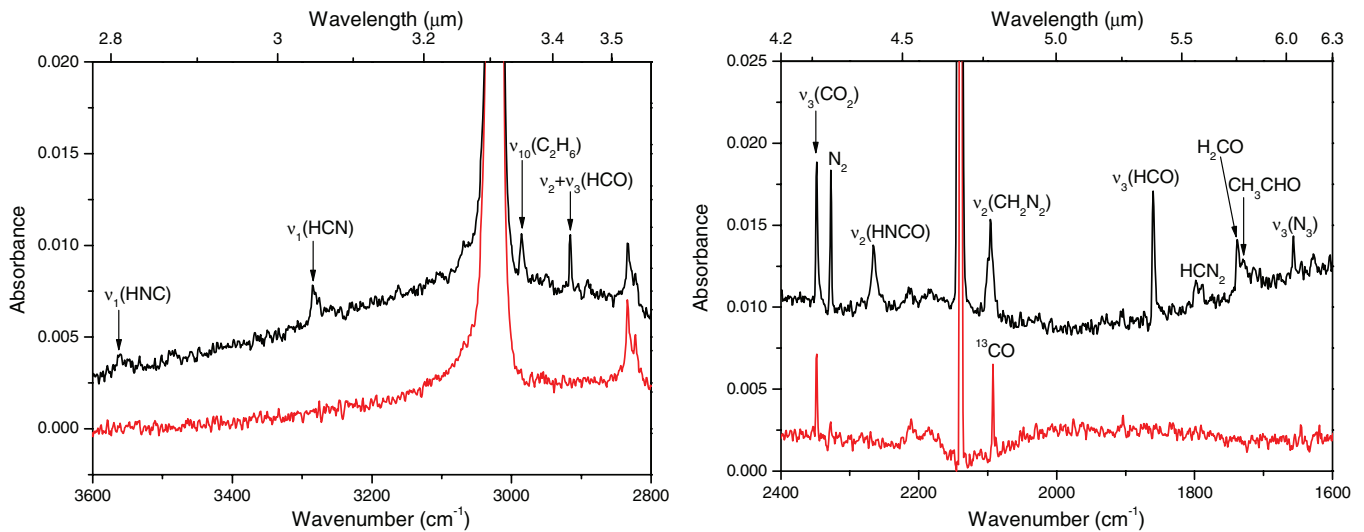


Figure 2. Infrared spectra of the ternary N_2 - CH_4 - CO ice before (lower trace) and after (upper trace) the electron irradiation at 10 K. The assignments of the newly formed species are compiled in Table 1.

(A color version of this figure is available in the online journal.)

Table 1

Infrared Absorption Features Recorded before and after Irradiation of the Ternary N_2 - CH_4 - CO (60:1:1) Ices at 10 K

Irradiation at 10 K		Reference	Literature Assignment	
Before (cm^{-1})	After (cm^{-1})		(cm^{-1})	Carrier
~4320	...	1/2	~4300/4328	$\nu_3 + \nu_4(CH_4)$
4252	...	3	4251	$2\nu_1(CO)$
~4218	...	1/2	~4200/4219	$\nu_1 + \nu_4(CH_4)$
...	3562	4	3565	$\nu_1(HNC)$
...	3285	4	3285	$\nu_1(HCN)$
~3025	...	1/2	~3005/3031	$\nu_3(CH_4)$
...	2985	1	2975	$\nu_{10}(C_2H_6)$
...	2916 ^a	5	2945	$\nu_2 + \nu_3(HCO)$
~2830	...	1/2	~2815/2835	$\nu_2 + \nu_4(CH_4)$
2348 ^b	2348	3	2346	$\nu_3(CO_2)$
...	2266	4	2266	$\nu_2(HNCO)$
2140	...	3	2136	$\nu_1(CO)$
...	2096 ^c	4	2096	$\nu_2(CH_2N_2)$
2092	...	3	2091	$\nu_1(^{13}CO)$
...	1860	4	1861	$\nu_3(HCO)$
...	1800, 1789	4	1798	HCN_2
...	1738	4	1736	$\nu_2(H_2CO)$
...	1728	4,6	1728	$\nu_4(CH_3CHO)$
...	1656	7	1657	$\nu_3(N_3)$
...	1408	4	1407	$\nu_3(CH_2N_2)$
~1306	...	1/2	~1300/1306	$\nu_4(CH_4)$
...	1090	4	1089	$\nu_2(HCO)$
...	611	1	608	$\nu_2(CH_3)$

Notes.

^a Tentatively assigned from a laser-induced fluorescence study (Sappety & Crosley 1990).

^b Residual impurity.

^c Including about 4% or less contribution of $\nu_3(HCN)$.

References. (1) Bennett et al. 2006; (2) Bohn et al. 1994; (3) Jamieson et al. 2006; (4) Moore & Hudson 2003; (5) Sappety & Crosley 1990; (6) Bennett et al. 2005; (7) Jamieson & Kaiser 2007.

new absorption features, the carriers of which are listed along with the vibrational assignments in Table 1. The array of products is identified to be more or less cumulative of what to expect from two binary ices under ionizing radiation, N_2 - CH_4

and CO - CH_4 (Moore & Hudson 2003; Bennett et al. 2005). Nitrogen and oxygen-bearing isocyanic acid (HNCO) is also found in electron-irradiated ternary ices as in proton-irradiated ices (Moore & Hudson 2003). Unlike the previous N_2 - CO ice study (Kim et al. 2011), any nitrogen oxides (N_xO_y), isocyanato radical (OCN), or diazirinone (N_2CO) are collectively absent in the current irradiated ices.

Reminiscent of pure ice processing, the azide radical (N_3) emerged at 1656 cm^{-1} , the methyl (CH_3) radical and ethane (C_2H_6) at 611 and 2985 cm^{-1} , and carbon dioxide (CO_2) at 2348 cm^{-1} (Table 1). The new species diazomethane (CH_2N_2) was identified with two absorptions at 2096 cm^{-1} (ν_2) and 1408 cm^{-1} (ν_3), which arose to their maximum intensities within the initial 30 minutes of irradiation (Moore & Pimentel 1964). The exposure also triggered a fragment HCN_2 radical to emerge at 1800 and 1789 cm^{-1} (Moore & Hudson 2003; Wu et al. 2012). Notable but weak transitions of hydrogen cyanide (HCN) and hydrogen isocyanide (HNC) isomer pairs were found at 3285 cm^{-1} (ν_1) and 3562 cm^{-1} (ν_1), respectively. Acetylene (C_2H_2) is suspected near 3280 cm^{-1} but below the current detection limit. Furthermore, the presence of $\nu_3(HCN)$ at 2096 cm^{-1} cannot be verified due to the overlying $\nu_2(CH_2N_2)$ feature, but can be inferred at 4% or less of the diazomethane level (Moore & Hudson 2003; Wu et al. 2012).

Meanwhile, the formyl radical (HCO) has at least two absorptions identified at 1860 cm^{-1} (ν_3) and 1090 cm^{-1} (ν_2), which arose to their maximum intensities within the initial 10 minutes of irradiation; the current exposure further allowed a third transition to appear at 2916 cm^{-1} , attributable to a combination of ν_2 and ν_3 (Figure 2). This combination band was previously recorded in a laser-induced fluorescence study of HCO radical (Sappety & Crosley 1990), but not in either of the photolyzed hydrogen iodide (HI)- CO ices (Ewing et al. 1960) or proton-irradiated N_2 - CH_4 - CO ices (Moore & Hudson 2003). Analogous to those initially identified in a binary CH_4 and CO ice (Moore & Hudson 2003), formaldehyde (H_2CO) and acetaldehyde (CH_3CHO) were found to appear side by side at about 1738 and 1728 cm^{-1} in the current irradiated ices. Finally, a steady rising feature at 2266 cm^{-1} could be attributed to the ν_2 of isocyanic acid (HNCO; Moore & Hudson 2003; Figure 2).

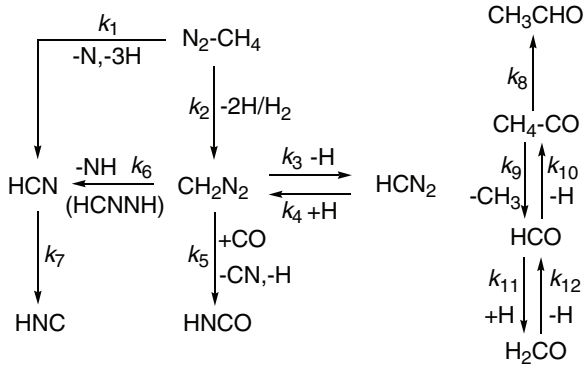


Figure 3. Reaction schemes used to fit the temporal profiles of the species produced during the radiation exposure of the ternary ice mixture of nitrogen, methane, and carbon monoxide ices at 10 K.

4. DISCUSSION

Along with isocyanic acid (HNCO), multiple products were identified in electron-irradiated $\text{N}_2\text{-CH}_4\text{-CO}$ ices, which are cumulative of what to expect from the simple methane, nitrogen, and carbon monoxide ices as well as from the binary ices under ionizing radiation, $\text{N}_2\text{-CH}_4$ and CO-CH_4 (Table 1).

This section is dedicated to gaining mechanistic insights into how these species could have formed in the simulation of KBO volatile ternary ices under ionizing radiation. For this purpose, two kinetic reaction schemes were developed to fit the temporal (integrated infrared absorptions) profiles of the species produced during the radiation exposure (Figures 3 and 4). A system of coupled differential equations was numerically solved (Frenklach et al. 1992; 2007), resulting in sets of rate constants ($k_1\text{-}k_7, k_9\text{-}k_{14}$; Table 2). For comparison, the temporal formyl radical (HCO) was also fit for the intermediate B of the consecutive $\text{A} \rightarrow \text{B} \rightarrow \text{C}$ scheme as detailed below. The formation of acetaldehyde (CH_3CHO) is uncoupled to proceed and fit (k_8) in the one-step $\text{A} \rightarrow \text{C}$ reaction scheme, as elucidated earlier (Bennett et al. 2005).

First, we will briefly elaborate the formation of simple molecules. As in Jamieson & Kaiser (2007) and references therein, the azide radical (N_3) at 1656 cm^{-1} is suggested to form via two-step processes involving the bond cleavage of a nitrogen molecule and the subsequent reaction of suprathreshold nitrogen $\text{N}(^2D/4S)$ atoms with a molecular nitrogen (reactions (1) and (2)):

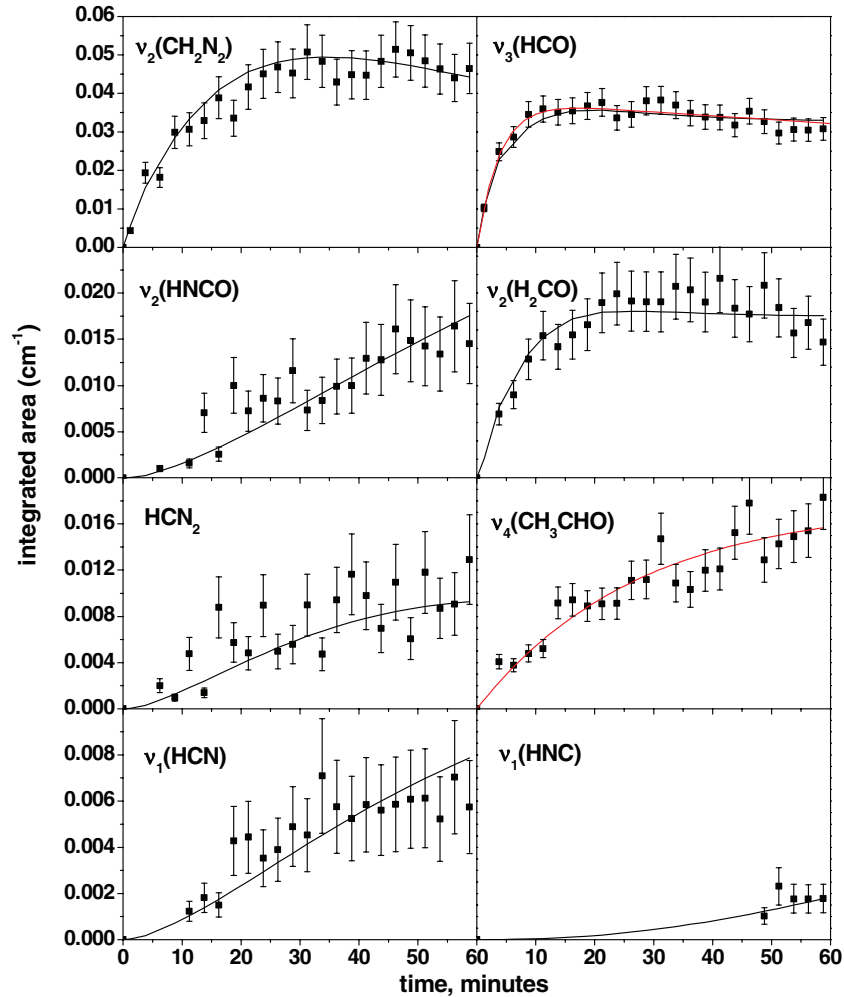
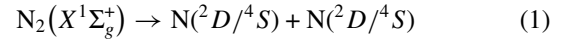


Figure 4. Fit of the temporal evolution of selected species produced during the radiation exposure at 10 K. The fit (black trace) of the $\nu_3(\text{HCO})$ is further compared with an analytical fit (red trace) for a potential intermediate B of the consecutive $\text{A} \rightarrow \text{B} \rightarrow \text{C}$ reaction scheme. The derived kinetic values are compiled in Table 2 and discussed in Section 4.

(A color version of this figure is available in the online journal.)

Table 2

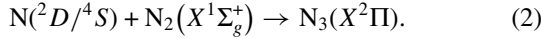
Rate Constants Derived via Iterative Solution of the Temporal Traces of Newly Formed Species Utilizing Reaction Schemes as Compiled in Figure 3

Reaction	Rate Constant
Pathways for N ₂ –CH ₄ decomposition in CO	
N ₂ –CH ₄ → HCN + 3H/N	$k_1 = 1.7 \times 10^{-6}$ a
N ₂ –CH ₄ → CH ₂ N ₂ + 2H/H ₂	$k_2 = 9.7 \times 10^{-4}$ a
CH ₂ N ₂ → HCN ₂ + H	$k_3 = 1.4 \times 10^{-4}$ a
HCN ₂ + H → CH ₂ N ₂	$k_4 = 5.8 \times 10^{-4}$ b
CH ₂ N ₂ + CO → HNCO + H/CN	$k_5 = 1.2 \times 10^{-4}$ b
CH ₂ N ₂ → HCN + NH	$k_6 = 6.4 \times 10^{-5}$ a
HCN → HNC	$k_7 = 1.2 \times 10^{-4}$ a
Pathways for CH ₄ –CO decomposition in N ₂	
CH ₄ –CO → CH ₃ CHO	$k_8 = 6.1 \times 10^{-4}$ a
CH ₄ –CO → HCO + CH ₃	$k_9 = 2.8 \times 10^{-3}$ a
HCO → CO + H	$k_{10} = 1.5 \times 10^{-4}$ a
HCO + H → H ₂ CO	$k_{11} = 5.4 \times 10^{-3}$ b
H ₂ CO → HCO + H	$k_{12} = 1.0 \times 10^{-2}$ a
H ₂ CO → X	$k_{13} = 1.4 \times 10^{-3}$ a
X → H ₂ CO	$k_{14} = 1.2 \times 10^{-3}$ a

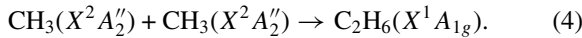
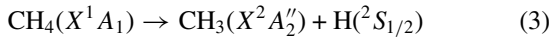
Notes. Rate constant (k_8) and initial concentration ($A_0 = (1.8 \pm 0.2) \times 10^{-2}$ cm⁻¹) of the first-order fit discussed in Section 4.

^a Units in s⁻¹ (first order).

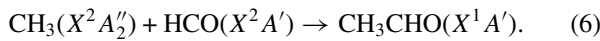
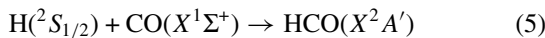
^b Units in cm s⁻¹ (second order).



As in Bennett et al. (2006), the methyl (CH₃) radical at 611 cm⁻¹ forms upon the cleavage of carbon–hydrogen bond of methane (CH₄) (reaction (3)), invoking the radical–radical recombination to ethane (C₂H₆) at 2985 cm⁻¹ (reaction (4)):



Released by reaction (3), hydrogen atoms can carry excess energies to overcome the entrance barrier of the reaction with CO (reaction (5)), thus unleashing the pathways for CH₄–CO decomposition (Bennett et al. 2005) in N₂. Depending on the reactant geometries inside a matrix cage, methyl (CH₃) and the formyl (HCO) radical pair can then recombine barrierlessly to form acetaldehyde (CH₃CHO) in reaction (6) (Figure 3):



The formyl radical (HCO) was found to form fast at $k_9 = 2.8 \times 10^{-3}$ s⁻¹ and to reverse back to CO at $k_{10} = 1.5 \times 10^{-4}$ s⁻¹ in response to a decay toward higher radiation exposure (Figure 4, Table 2). For comparison, the temporal growth of HCO was also fit for the intermediate B of consecutive (A → B → C) reaction scheme (7) and overlaid in Figure 4:

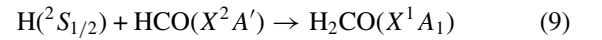
$$[\text{B}]_t = \frac{[\text{A}]_0 k_a}{k_a - k_b} (e^{-k_b t} - e^{-k_a t}). \quad (7)$$

The following values were accordingly derived: $k_a = (4.4 \pm 0.3) \times 10^{-3}$ s⁻¹, $k_b = (4.9 \pm 0.4) \times 10^{-5}$ s⁻¹, and $A_0 = (3.8 \pm 0.1) \times 10^{-2}$ cm⁻¹, equivalent to the initial rise (k_a), the subsequent decay (k_b), and the initial concentration (A_0) for the

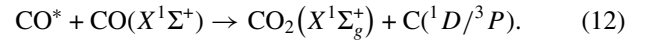
case of $k_a > k_b$ (Bennett & Kaiser 2005 and references therein). Recall that the initial rise (k_a) can also be the formation rate of the formyl radical, $(3.8 \pm 0.6) \times 10^{-3}$ s⁻¹, found in the binary CO–CH₄ ice study (Bennett et al. 2005). The temporal absorptions of $\nu_3(\text{CH}_3\text{CHO})$ at 1728 cm⁻¹ were accordingly deconvoluted with Gaussians from the adjacent $\nu_2(\text{H}_2\text{CO})$ at 1738 cm⁻¹, allowing the profile to be fit in a pseudo-first-order (A → C) at $k_8 = (6.1 \pm 1.3) \times 10^{-4}$ s⁻¹ (reaction (8); Figure 4):

$$[\text{C}]_t = [\text{A}]_0 (1 - e^{-k_8 t}). \quad (8)$$

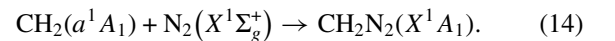
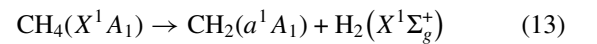
Indeed, a comparable rate $(5.4 \pm 2.3) \times 10^{-4}$ s⁻¹ of CH₃CHO formation was also found in the binary ice study (Table 2; Bennett et al. 2005). Furthermore, the stepwise (suprathermal) hydrogenation of carbon monoxide (CO) continued through the intermediate (HCO) to formaldehyde (H₂CO) and even to an unidentified X (reactions (9) and (10)) with equally rapid forward rates and backward rates (k_{11} – k_{14}) (Table 2):



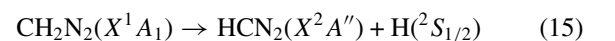
Likewise, carbon dioxide (CO₂) at 2348 cm⁻¹ is suggested to form in a multifold of CO dissociation, one of which involves an electronically excited carbon monoxide CO(A¹Π/a³Π) in the reaction with a neighboring CO (Jamieson et al. 2006; reactions (11) and (12)):

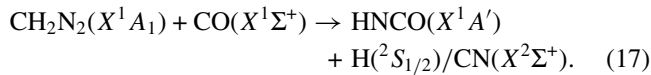
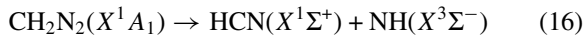


Second, we will detail the formation of complex molecules. In the initial pathways for N₂–CH₄ decomposition in CO (Figure 3), the ionizing radiation leads to the formation of hydrogen cyanide (HCN) and diazomethane (CH₂N₂) with rates of $k_1 = 1.7 \times 10^{-6}$ s⁻¹ and $k_2 = 9.7 \times 10^{-4}$ s⁻¹, respectively (Table 2). The difference of formation rates might well hinge on that of electronic energy transfers required to dissociate N₂ (~9.8 eV; reaction (1)) or CH₄ (~4.5 eV; Bennett et al. 2006). Methylene carbene (CH₂), possibly produced in reaction (13) or via radiolysis of the methyl radical, could then react with a neighboring nitrogen molecule to yield diazomethane (CH₂N₂) (reaction (14)). Hydrogen atoms also released in this way can be suprathermal (non equilibrium), carrying excess energies of up to a few eV (Bennett et al. 2006):



The facile growth (k_2) of $\nu_2(\text{CH}_2\text{N}_2)$ was captured in a pseudo-first-order kinetics, particularly within the initial 30 minutes of irradiation (Figure 4); a particular attention was paid to suppress any influence of natural isotopomer ¹³CO at 2092 cm⁻¹ within margins of error bars set for the temporal integrated area (cm⁻¹) of $\nu_2(\text{CH}_2\text{N}_2)$ (Figure 4). As outlined in the reaction schemes of Figure 3, three channels were proposed to compete in the diazomethane (CH₂N₂) decomposition (reactions (15)–(17)):





The formation of the HCN_2 radical (reaction (15)) was found to proceed at $k_3 = 1.4 \times 10^{-4} \text{ s}^{-1}$ and to replenish back CH_2N_2 at $k_4 = 5.8 \times 10^{-4} \text{ cm s}^{-1}$ (Table 2). As Moore & Hudson (2003) suggested, channel (16) would be likely to pass through an intermediate (HCNNH ; Figure 3), resulting in a higher-order fit of $k_6 = 6.4 \times 10^{-5} \text{ s}^{-1}$ (Figure 4). Finally, a steady rise of isocyanic acid (HNCO) was monitored at 2266 cm^{-1} , likely driving CH_2N_2 signals to level out at higher radiation doses (Figure 4). Accordingly, a net reaction (17) was raised for this conversion to a nominal second-order rate (k_5) of $1.2 \times 10^{-4} \text{ cm s}^{-1}$.

5. CONCLUSION AND ASTROPHYSICAL IMPLICATIONS

Space weathering of KBO surfaces was simulated in the current case study by exposing nitrogen (N_2)-rich methane (CH_4) and carbon monoxide (CO) ices to ionizing radiation of energetic electrons found in magnetospheres of giant planets or in the track of GCR particles (Bennett et al. 2005; Barnett et al. 2012). Using online and in situ FT-IR spectroscopy, the radiation-induced formation of new species at 10 K was monitored and compared with those found in 800 keV proton trajectories (Table 1; Moore & Hudson 2003). Nitrogen-bearing products were found to be of hydrogen cyanide (HCN), hydrogen isocyanide (HNC), diazomethane (CH_2N_2), and its fragment (HCN_2). Oxygen-bearing products were of acetaldehyde (CH_3CHO), formyl radical (HCO), and formaldehyde (H_2CO). Isocyanic acid (HNCO) was also present, bearing both nitrogen and oxygen elements, while species of nitrogen oxides (N_xO_y), isocyanato radical (OCN), or diazirinone (N_2CO) were collectively absent in electron-irradiated ices.

In light of the product distribution, two kinetic schemes (Figure 3, Table 2) were developed to fit the temporal profiles of the products (Figure 4) in the destruction paths of impinging electrons (Bennett et al. 2005; Kim et al. 2011). In light of energetics, about 4.5 eV electronic energies could be transferrable to initial ices allowing for methyl radical $\text{CH}_3(X^2A_2')$ and methylene carbene $\text{CH}_2(a^1A_1)$ to form (reactions (3) and (13)). Also released from both channels could be suprathermal hydrogen atoms having excess energies of a few eV. The reactivity of non-equilibrium fragments was also expressed in a

pseudo-first-order reaction of forming acetaldehyde (CH_3CHO) (6) and diazomethane (CH_2N_2) (14). A successive ionizing interaction turned favorable on the formation of isocyanic acid (HNCO) rather than on the HCN/HNC isomer pair. In this respect, we further suggest a spectroscopic field survey toward actual KBO surface ices aiming to correlate the space weathering with relative abundances of these organic acids as found in the current case study.

This work was supported by the US National Science Foundation (NSF-CRC CHE-0627854). We acknowledge Dr. C. S. Jamieson (University of Hawaii) for experimental contributions.

REFERENCES

- Alvarez-Candal, A., Pinilla-Alonso, N., Licandro, J., et al. 2011, *A&A*, **532**, A130
- Barnett, I. L., Lignell, A., & Gudipati, M. S. 2012, *ApJ*, **747**, 13
- Bennett, C. J., Jamieson, C., Mebel, A. M., & Kaiser, R. I. 2004, *Phys. Chem. Chem. Phys.*, **6**, 735
- Bennett, C. J., Jamieson, C. S., Osamura, Y., & Kaiser, R. I. 2005, *ApJ*, **624**, 1097
- Bennett, C. J., Jamieson, C. S., Osamura, Y., & Kaiser, R. I. 2006, *ApJ*, **653**, 792
- Bennett, C. J., & Kaiser, R. I. 2005, *ApJ*, **635**, 1362
- Bohn, R. B., Sandford, S. A., Allamandola, L. J., & Cruikshank, D. P. 1994, *Icarus*, **111**, 151
- Brown, M. E., Schaller, E. L., & Fraser, W. C. 2011, *ApJ*, **739**, L60
- Cooper, J. F., Christian, E. R., Richardson, J. D., & Wang, C. 2003, *Earth Moon Planets*, **92**, 261
- Douté, S., Schmitt, B., Quirico, E., et al. 1999, *Icarus*, **142**, 421
- Ewing, G. E., Thompson, W. E., & Pimentel, G. C. 1960, *J. Chem. Phys.*, **32**, 927
- Frenklach, M., Packard, A., & Feeley, R. 2007, in Modeling of Chemical Reactions, ed. R. W. Carr (Elsevier Series Comprehensive Chemical Kinetics, Vol. 42; Amsterdam: Elsevier), 243
- Frenklach, M., Wang, H., & Rabinowitz, M. J. 1992, *Prog. Energy Combust. Sci.*, **18**, 47
- Fulvio, D., Guglielmino, S., Favone, T., & Palumbo, M. E. 2010, *A&A*, **511**, A62
- Grundy, W. M., Young, L. A., Stansberry, J. A., et al. 2010, *Icarus*, **205**, 594
- Gulbis, A. 2011, *Nature*, **478**, 464
- Jamieson, C., Mebel, A. M., & Kaiser, R. I. 2006, *ApJS*, **163**, 184
- Jamieson, C. S., & Kaiser, R. I. 2007, *Chem. Phys. Lett.*, **440**, 98
- Kim, Y. S., Zhang, F., & Kaiser, R. I. 2011, *Phys. Chem. Chem. Phys.*, **13**, 15766
- Luu, J., & Jewitt, D. 1996, *AJ*, **112**, 2310
- Moore, C. B., & Pimentel, G. C. 1964, *J. Chem. Phys.*, **40**, 342
- Moore, M. H., & Hudson, R. L. 2003, *Icarus*, **161**, 486
- Quirico, E., Duoté, S., Schmitt, B., et al. 1999, *Icarus*, **139**, 159
- Sappety, A. D., & Crosley, D. R. 1990, *J. Chem. Phys.*, **93**, 7601
- Schaller, E. L., & Brown, M. E. 2007, *ApJ*, **659**, L61
- Sicardy, B., Ortiz, J. L., Assafin, M., et al. 2011, *Nature*, **478**, 493
- Tegler, S. C., Cornelison, D. M., Grundy, W. M., et al. 2010, *ApJ*, **725**, 1296
- Tegler, S. C., Romanishin, W., & Consolmagno, G. 2003, *ApJ*, **599**, L49
- Wu, Y.-J., Wu, C. Y. R., Chou, S.-L., et al. 2012, *ApJ*, **746**, 175